THE JOURNAL OF BIOLOGICAL CHEMISTRY VOL. 290, NO. 17, pp. 11032–11040, April 24, 2015

Targeted Disruption of Ig-Hepta/Gpr116 Causes Emphysema-like Symptoms That Are Associated with Alveolar Macrophage Activation*

Received for publication, February 26, 2015 Published, JBC Papers in Press, March 16, 2015, DOI 10.1074/jbc.M115.648311

Donna Maretta Ariestanti, Hikaru Ando, Shigehisa Hirose, and Nobuhiro Nakamura[1]

From the Department of Biological Sciences, Tokyo Institute of Technology, 4259-B13 Nagatsuta-cho, Midori-ku, Yokohama 226-8501, Japan

Background: Ig-Hepta knock-out mice exhibit emphysema-like symptoms, but their pathogenesis remains unclear.
Results: In Ig-Hepta knock-out mice, alveolar macrophages are activated and release matrix metalloproteinases through reactive oxygen species-mediated nuclear factor-κB activation.
Conclusion: Ig-Hepta is likely to negatively regulate macrophage function and inflammation in the alveoli.
Significance: These findings reveal a novel mechanism for maintaining lung homeostasis and immune regulation.

Ig-Hepta/GPR116 is a member of the G protein-coupled receptor family predominantly expressed in the alveolar type II epithelial cells of the lung. Previous studies have shown that Ig-Hepta is essential for lung surfactant homeostasis, and loss of its function results in high accumulation of surfactant lipids and proteins in the alveolar space. Ig-Hepta knock-out (*Ig-Hepta*$^{-/-}$) mice also exhibit emphysema-like symptoms, including accumulation of foamy alveolar macrophages (AMs), but its pathogenic mechanism is unknown. Here, we show that the bronchoalveolar lavage fluid obtained from *Ig-Hepta*$^{-/-}$ mice contains high levels of inflammatory mediators, lipid hydroperoxides, and matrix metalloproteinases (MMPs), which are produced by AMs. Accumulation of reactive oxygen species was observed in the AMs of *Ig-Hepta*$^{-/-}$ mice in an age-dependent manner. In addition, nuclear factor-κB (NF-κB) is activated and translocated into the nuclei of the AMs of *Ig-Hepta*$^{-/-}$ mice. Release of MMP-2 and MMP-9 from the AMs was strongly inhibited by treatment with inhibitors of oxidants and NF-κB. We also found that the level of monocyte chemotactic protein-1 is increased in the embryonic lungs of *Ig-Hepta*$^{-/-}$ mice at 18.5 days postcoitum, when AMs are not accumulated and activated. These results suggest that Ig-Hepta plays an important role in regulating macrophage immune responses, and its deficiency leads to local inflammation in the lung, where AMs produce excessive amounts of reactive oxygen species and up-regulate MMPs through the NF-κB signaling pathway.

Pulmonary emphysema is a type of chronic obstructive pulmonary disease (COPD),[2] a major cause of worldwide morbidity and mortality (1). Emphysema is characterized by abnormal enlargement of airspaces and destruction of alveolar walls. These structural changes are associated with decreased lung elastic recoil, increased lung compliance, and lung hyperinflation. Cigarette smoking is a major cause of emphysema, but there are several environmental (*e.g.* second hand smoke and air pollution) and genetic (*e.g.* α1-antitrypsin deficiency) contributors to the development of this (2). In the alveoli, alveolar macrophages (AMs) serve as the first line of host defense against invading pathogens but play important roles in the pathogenesis of emphysema. AMs accumulate and become the dominant leukocyte population in the alveoli of emphysema patients and smokers (3). They release various inflammatory mediators, including tumor necrosis factor (TNF)-α, monocyte chemotactic protein (MCP)-1, and reactive oxygen species (ROS), which promote pulmonary inflammation (4–6). It has been shown that ROS induce expression of macrophage matrix metalloproteinases (MMPs), including MMP-2, MMP-9, and MMP-12, through activation of the transcription factor nuclear factor-kappa B (NF-κB) (7–11). MMPs are a family of Ca^{2+}-activated Zn^{2+}-dependent proteases that degrade the extracellular matrix, such as collagens, elastins, and gelatin (12). Imbalance between MMPs and their endogenous inhibitors, tissue inhibitors of metalloproteinases (TIMPs), is thought to cause emphysematous destruction of the lung parenchyma (13). Although a number of studies have used animal models (*e.g.* smoke-exposed mice and gene knock-out mice) to study the pathogenesis of emphysema, none of them accurately reproduce the human disease condition. The reason for this problem is probably due to the differences among species and strains in lung anatomy and in response to lung injury (14, 15). Therefore, the use and identification of an appropriate model will be essential to address specific concerns related to the pathogenesis and treatment of emphysema.

* This work was supported by Grants-in-aid for scientific research 21026010, 24117707, and 22770123 from the Ministry of Education, Culture, Sports, Sciences, and Technology of Japan and the Japan Society for the Promotion of Science.

[1] To whom correspondence should be addressed. Tel.: 81-45-924-5726; Fax: 81-45-924-5824; E-mail: nnakamur@bio.titech.ac.jp.

[2] The abbreviations used are: COPD, chronic obstructive pulmonary disease; AM, alveolar macrophage; MCP, monocyte chemotactic protein; ROS, reactive oxygen species; MMP, matrix metalloproteinase; NF-κB, nuclear factor-κB; TIMP, tissue inhibitor of metalloproteinase; SP, surfactant protein; BALF, bronchoalveolar lavage fluid; dpc, days post coitum; H_2DCFDA, 2′,7′-dichlorodihydrofluorescein diacetate; LPO, lipid hydroperoxide; CCL, CC chemokine ligand; CXCL, CXC chemokine ligand; LPO, lipid hydroperoxide.

Pulmonary surfactant plays an essential role in reducing the surface tension of the air-liquid interface of the alveoli, thereby preventing alveolar collapse (atelectasis) during expiration (16). A growing body of evidence has suggested that pulmonary surfactant is correlated with the development of COPD. Pulmonary surfactant is a surface-active lipoprotein complex secreted by the alveolar type II cells. Exposure of pulmonary surfactant to air pollution and oxidants results in peroxidation of surfactant lipids and oxidation of surfactant proteins, leading to inactivation of pulmonary surfactant, alveolar collapse, and impaired gas exchange (17–19). Genetic mutations in the surfactant protein (SP)-C gene is associated with interstitial lung disease, including emphysema (20, 21). Deficiency of SP-C induces endoplasmic reticulum stress in the alveolar type II cells, which promotes apoptotic and proinflammatory signaling pathways (22). Mice lacking SP-D develop emphysema with remodeling of the lung parenchyma, progressive accumulation of foamy AMs and surfactant components, and excessive proinflammatory response (23, 24). Mice lacking ATP-binding cassette A3 (ABCA3), a lipid transporter required for surfactant lipid synthesis, exhibit abnormal surfactant homeostasis, emphysema, and respiratory distress (25). Given the evidence, tightly controlled homeostasis of pulmonary surfactant plays an essential protective role in the development of emphysema and its regulators could be potential drug targets for this disease.

Ig-Hepta is a member of the adhesion class of G protein-coupled receptors. Ig-Hepta was first identified as an orphan receptor predominantly expressed in the lung (26). Recent studies have reported that Ig-Hepta is highly expressed in the alveolar type II cells and essential for homeostasis of pulmonary surfactant. Mice deficient in Ig-Hepta exhibit massive accumulation of pulmonary surfactant in the alveoli due to abnormal synthesis and catabolism of surfactant lipids and proteins in the alveolar type II cells (27–29). Ig-Hepta knock-out (*Ig-Hepta*$^{-/-}$) mice also exhibit emphysema-like symptoms with enlarged alveoli, accumulation of foamy AMs, and increased expression of MMP-12 (27). We therefore hypothesized that *Ig-Hepta* would be of potential importance in the pathogenesis of emphysema and that *Ig-Hepta*$^{-/-}$ mice would be a new potential model of emphysema. In this study, we show that AMs of *Ig-Hepta*$^{-/-}$ mice are highly activated and release several cytokines/chemokines and ROS. Excess amounts of ROS induce the secretion of MMP-2 and MMP-9 from AMs through activation of NF-κB. These observations suggest that Ig-Hepta plays an important role in lung homeostasis by regulating immune regulation in the alveoli.

EXPERIMENTAL PROCEDURES

Animals—Ig-Hepta$^{-/-}$ mice were described previously (27). The animal protocols and procedures were approved by the Institutional Animal Care and Use Committee of the Tokyo Institute of Technology.

Extraction of Bronchoalveolar Lavage Fluid (BALF) and Isolation of AMs—BALF was obtained according to methods described previously with modifications (27, 30). Mice were anesthetized with 2% isoflurane (Wako Pure Chemicals, Osaka, Japan) by inhalation. Three alveolar lavages (1 ml of phosphate-buffered saline (PBS) each) were performed for each mouse. For some experiments, BALF from several mice was pooled to increase the yield of AMs. AMs were isolated by differential attachment to tissue culture dishes at 37 °C. BALF was centrifuged at 1,000 × *g* for 5 min at 20 °C. Pelleted cells were resuspended in RPMI 1640 medium (Sigma-Aldrich) and were then transferred to cell culture dishes. After incubation for 1 h at 37 °C, the medium was replaced with a fresh one to remove nonadherent cells. Adherent AMs were used for experiments.

Cytokine Array Analysis—BALF samples were cleared by centrifugation at 1,000 × *g* for 10 min at 4 °C followed by ultracentrifugation at 240,000 × *g* for 30 min at 4 °C in an SW41Ti rotor (Beckman Coulter, Sunnyvale, CA). To obtain cytokine/chemokines secreted from AMs, AMs isolated from three mice were incubated in 1 ml of serum-free RPMI 1640 medium for 8 h at 37 °C. The medium was then cleared by centrifugation at 60,000 rpm in a TLA100.3 rotor (Beckman Coulter) for 20 min. To prepare the lysates of embryonic lung, lungs from three embryonic mice (18.5 days post coitum (dpc)) were homogenized in PBS containing 1% Triton X-100 and protease inhibitors (10 μM leupeptin, 1 μM pepstatin A, 5 μg/ml aprotinin, 5 mM EDTA, and 1 mM phenylmethylsulfonyl fluoride) and then centrifuged at 60,000 rpm in a TLA100.3 rotor for 20 min. The supernatants were used as samples for Proteome Profiler Mouse Cytokine Array Panel A (R&D Systems, Minneapolis, MN), following the manufacturer's instructions. The signals were visualized with the chemiluminescent detection reagent Luminata Forte (Millipore, Bedford, MA) and were captured using ImageQuant LAS 4000 mini, a chemiluminescent image analyzer (GE Healthcare). Individual signal intensities were evaluated using ImageJ analysis software (National Institutes of Health, Bethesda, MD). Results are reported as average signal intensities based on pixel density.

Detection of Intracellular ROS—Accumulation of ROS in AMs was detected with the fluorescent probe 2′,7′-dichlorodihydrofluorescein diacetate (H_2DCFDA; Biotium, Hayward, CA). Freshly isolated AMs were gently rinsed with PBS three times and were then incubated with 10 μM H_2DCFDA in RPMI 1640 without phenol red for 30 min at 37 °C. After three times washing with PBS, the cells were fixed with 4% paraformaldehyde in PBS and stained with anti-CD68 antibody (AbD Serotec, Kidlington, Oxford, UK) at a dilution of 1:100 as described below. Images were captured with a TSC-SPE laser confocal microscope (Leica, Wetzlar, Germany).

Measurement of Lipid Hydroperoxide (LPO)—The levels of LPO were measured with the LPO assay kit (Cayman Chemical, Ann Arbor, MI) according to the manufacturer's instructions. BALF and remaining lungs after lavaged were isolated and homogenized in PBS on ice. After centrifugation of the sample at 3,000 × *g* for 10 min at 4 °C, LPO was immediately extracted from the sample into chloroform and assayed according to the manufacturer's protocols.

Immunofluorescence Staining—AMs on coverslips were fixed with 4% paraformaldehyde in PBS for 10 min, permeabilized with 0.2% Triton X-100 in PBS for 10 min, and blocked with 5% fetal bovine serum for 30 min at room temperature. The cells were incubated for 2 h at room temperature with anti-NF-κB p65 antibody (sc-109; Santa Cruz Biotechnology, Inc.) at a 1:50

dilution in PBS containing 5% fetal bovine serum. The cells were then incubated for 1 h at room temperature with Alexa Fluor 488-labeled anti-rabbit IgG antibody (Molecular Probes, Inc., Eugene, OR). Images were captured with a TSC-SPE laser confocal microscope.

Gelatin Zymography—BALF from five mice was pooled, added with protease inhibitors (10 μM leupeptin, 1 μM pepstatin A, and 5 μg/ml aprotinin), and homogenized. After centrifugation at 20,000 $\times$ *g*, for 30 min at 4 °C, the supernatants were then concentrated with Amicon Ultra-30K centrifugal filter devices (Millipore). The samples (20 μg of proteins) were mixed with Tris-glycine SDS sample buffer (final concentrations: 63 mM Tris-HCl, pH 6.8, 10% glycerol, 2% SDS, and 0.0025% bromphenol blue) and applied without boiling to a 10% Novex Zymogram gelatin gel (a 10% Tris-glycine gel containing 0.1% gelatin; Life Technologies, Inc.). After electrophoresis, the gel was incubated with renaturing buffer (25% Triton X-100 in distilled water) for 30 min at room temperature to remove SDS from the gel, followed by developing buffer (50 mM Tris, pH 7.5, 200 mM NaCl, 5 mM $CaCl_2$, and 0.2% Brij 35) for 30 min at room temperature. The developing buffer was then replaced with a fresh one, and the gel was incubated for another 16–18 h at 37 °C. Subsequently, the gel was stained with 0.5% Coomassie Brilliant Blue R250 in 50% methanol and 10% acetic acid for 1 h and was then destained with 50% methanol and 10% acetic acid. The activities of MMPs were detected as clear bands against a blue background.

Treatment of AMs with Inhibitors in Vitro—AMs from Ig-Hepta$^{-/-}$ mice were pooled and placed in culture at a concentration of 5 $\times$ 10^5 cells/well in serum-free RPMI 1640 medium. The AMs were treated for 6 h at 37 °C with 20 mM *N*-acetyl-L-cysteine (Sigma-Aldrich), 200 μM pyrrolidine dithiocarbamate (Sigma-Aldrich), 50 μM parthenolide (Sigma-Aldrich), or 20 μM BAY 11–7082 (Wako Pure Chemical). After incubation, medium was removed, and the cells were washed and incubated with fresh medium including the reagents for 3 h. The medium was then collected, added with protease inhibitors (10 μM leupeptin, 1 μM pepstatin A, and 5 μg/ml aprotinin), and centrifuged at 1,000 $\times$ *g* for 10 min. The resulting supernatants were collected and used for gelatin zymography analysis.

Western Blot Analysis—Preparations of BALF samples were as described above. Remaining whole lung tissues were homogenized in 5 ml of PBS. The samples were added with protease inhibitors (10 μM leupeptin, 1 μM pepstatin A, 5 μg/ml aprotinin, 5 mM EDTA, and 1 mM phenylmethylsulfonyl fluoride) and 1% Triton X-100. Western blot analysis was performed according to previous methods with several modifications (27). Protein samples were separated by SDS-polyacrylamide gel electrophoresis and were then transferred onto an Immobilon FL polyvinyl difluoride membrane (Millipore) with a semidry blotter. After blocking with 5% nonfat milk in 150 mM NaCl, 10 mM Tris-Cl, pH 8, and 0.05% Tween 20 (TBS-T) for 1 h at room temperature, the membrane was incubated with primary antibodies overnight at 4 °C, followed by corresponding secondary antibodies conjugated to Alexa Fluor 680 (at a 1:10,000 dilution in TBS-T) for 1 h at room temperature. Signals were detected with the Odyssey infrared imaging system (LI-COR Biosciences, Lincoln, NE). The dilutions of the primary antibodies were as follows: NF-κB p65, 1:1,000; MMP2 (Abcam, Cambridge, MA), 1:1,000; MMP9 (Abcam), 1:1,000; IκB-α (sc-371, Santa Cruz Biotechnology), 1:200; histone H1 (MBL, Nagoya, Japan), 1:1,000; HSP90 (MBL), 1:1,000; Ig-Hepta N7, 1:2,000 (27); and F4/80 (CI:A3-1, AbD Serotec), 1:500.

Subcellular Fractionation—AMs from *Ig-Hepta*$^{-/-}$ mice were incubated in a 2$\times$ volume of buffer A (10 mM HEPES, pH 7.9, 10 mM KCl, 0.1 mM EDTA, 1.5 mM $MgCl_2$, 1 mM dithiothreitol, and 0.5 mM phenylmethylsulfonyl fluoride) for 15 min on ice. After adding Nonidet P-40 to a final concentration of 0.8%, the cells were gently vortexed for 10 s and then centrifuged at 800 $\times$ *g* for 10 min. The supernatant was cleared by centrifugation at 60,000 rpm in a TLA100.3 rotor for 20 min and then used as the cytosolic fraction. The pellet was washed with buffer A three times and then incubated in an equal volume of buffer C (20 mM HEPES, pH 7.9, 420 mM NaCl, 0.1 mM EDTA, 1.5 mM $MgCl_2$, 25% glycerol, 1 mM dithiothreitol, and 0.5 mM phenylmethylsulfonyl fluoride) for 30 min with vortex mixing at 10-min intervals. After centrifugation at 17,800 $\times$ *g* for 10 min, the resulting supernatant (nuclear fraction) was incubated with 0.1% SDS and then cleared by centrifugation at 60,000 rpm in a TLA100.3 rotor for 20 min.

Electrophoresis Mobility Shift Assay (EMSA)—EMSA was performed with the LightShift chemiluminescent EMSA kit (Promega, Madison, WI) according to the manufacturer's instructions. Nuclear extracts of AMs were mixed with 20 fmol of biotin-labeled consensus NF-κB oligonucleotide (5′-agttgaggggactttcccaggc-3′) in 20 μl of binding buffer (Promega) containing 2.5% glycerol, 5 mM $MgCl_2$, 50 ng/μl poly(dI·dC), and 0.05% Nonidet P-40. The reaction mixtures were incubated for 30 min at room temperature. For control experiments, an unlabeled consensus NF-κB oligonucleotide (4 pmol) was added to the reaction mixtures, or a biotin-labeled mutant oligonucleotide (5′-agttgaggcgactttcccaggc-3′) was used instead of the wild-type (WT) oligonucleotide.

Quantitative Real-time PCR—Total RNA was isolated with Isogen (Nippon Gene, Toyama, Japan) and used for synthesis of first strand DNA with SuperScript III reverse transcriptase (Life Technologies). Real-time PCR was performed with SYBR Premix Ex TaqII (Takara, Otsu, Japan) according to the manufacturer's instructions. The following primer sets were used: *Mmp2*, 5′-ggacaagtggtccgcgtaaa-3′ and 5′-ccgaccgttgaacaggaagg-3′; *Mmp9*, 5′-ctttgagtccggcagacaat-3′ and 5′-ttccagtaccaaccgtcctt-3′; and *Gapdh*, 5′-aggtcggtgtgaacggatt-3′ and 5′-tgccgtgagtggagtcatac-3′.

Statistical Analysis—Data are presented as the mean ± S.E. of at least three independent experiments. Statistical comparisons were performed with Student's *t* test, and a value of $p < 0.05$ was considered significant.

RESULTS

Alteration of Cytokine and Chemokine Profile in the Lung and AMs of Ig-Hepta$^{-/-}$ *Mice*—We examined the levels of secreted cytokines and chemokines by using an antibody array that could detect 40 different antigens. When the antibody arrays were incubated with cell-free BALF, high levels of cytokines and chemokines were detected in the BALF sample of *Ig-Hepta*$^{-/-}$

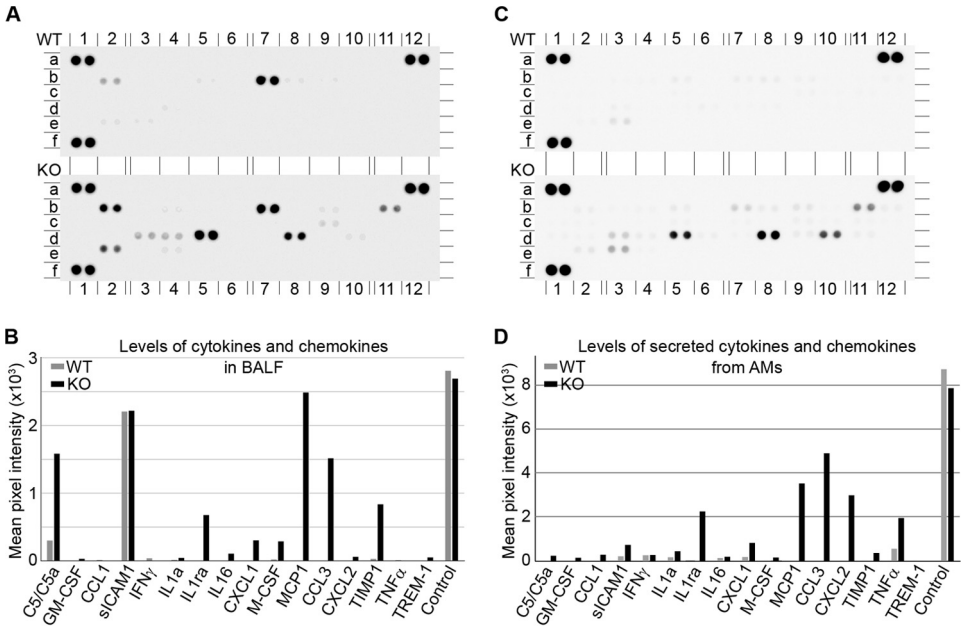

FIGURE 1. **Increased cytokine and chemokine expression in the BALF and AMs of *Ig-Hepta*$^{-/-}$.** *A* and *C*, Proteome Profiler Mouse Cytokine Arrays were used to detect cytokines and chemokines present in cell-free BALF (*A*) or those secreted from AMs (*C*) prepared from WT (*top*) and *Ig-Hepta*$^{-/-}$ (KO; *bottom*) mice. The identity of each spot is as follows. *a1*, *a12*, and *f1*, reference spots; *b1*, CXCL13; *b2*, complement component C5a; *b3*, G-CSF; *b4*, GM-CSF; *b5*, CCL1; *b6*, CCL11; *b7*, sICAM-1; *b8*, IFN-γ; *b9*, IL-1α; *b10*, IL-1β; *b11*, IL-1ra; *b12*, IL-2; *c1*, IL-3; *c2*, IL-4; *c3*, IL-5; *c4*, IL-6; *c5*, IL-7; *c6*, IL-10; *c7*, IL-13; *c8*, IL-12p70; *c9*, IL-16; *c10*, IL-17; *c11*, IL-23; *c12*, IL-27; *d1*, CXCL10; *d2*, CXCL11; *d3*, CXCL1; *d4*, M-CSF; *d5*, MCP-1; *d6*, CCL12; *d7*, CXCL9; *d8*, CCL3; *d9*, CCL4; *d10*, CXCL2; *d11*, CCL5; *d12*, CXCL12; *e1*, CCL17; *e2*, TIMP-1; *e3*, TNF-α; *e4*, TREM-1; *f12*, negative control. *B* and *D*, the signal intensity of each spot was quantified and shown in the bar graph. *Gray bar*, WT mice. *Filled bar*, *Ig-Hepta*$^{-/-}$ (KO) mice.

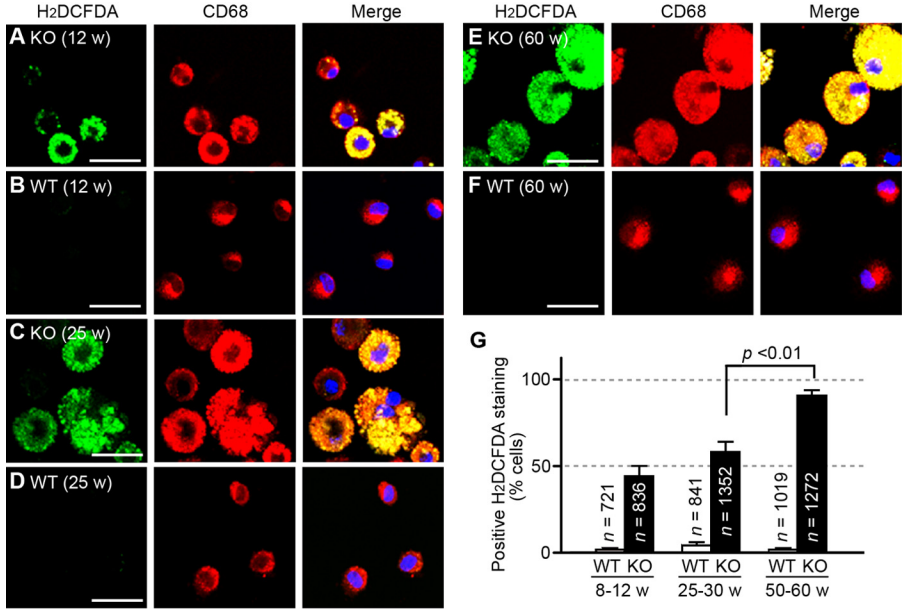

FIGURE 2. **ROS production in AMs.** *A–F*, AMs were isolated from *Ig-Hepta*$^{-/-}$ (KO; *A*, *C*, and *E*) and WT (*B*, *D*, and *F*) at 8–12, 25–30, and 50–60 weeks of age. The AMs were stained with H_2DCFDA for 30 min at 37 °C, followed by staining with anti-CD68 antibody, and then observed with a confocal microscope. Typical results obtained from 12-week-old (*A* and *B*), 25-week-old (*C* and *D*), and 60-week-old mice (*E* and *F*) are shown. H_2DCFDA staining (*green* in *left panels*), CD68 staining (*red* in *middle panels*), and overlays (*right panels*) are shown. *Bars*, 25 μm. *G*, bar graphs represent the percentage of AMs with H_2DCFDA staining quantified in randomly chosen views. Values are means ± S.E. (*error bars*) from three mice. The total numbers of cells counted are indicated *within* or *above* each *bar*.

mice, including MCP-1, complement component C5/C5a, CC chemokine ligand 3 (*CCL3*) (also known as MIP (macrophage inflammatory protein)-1α), TIMP-1, IL-1 receptor antagonist (*IL-1ra*), CXC chemokine ligand 1 (*CXCL1*), and M-CSF (Fig. 1, *A* and *B*). The expression of typical proinflammatory cytokines, such as TNFα, IL-1b and IL-6, and other cytokines/chemokines were very low or below the detection limit of the system. To examine whether these cytokines and chemokines were secreted from the AMs, antibody array analysis was performed on the supernatant of isolated AMs. A similar cytokine/chemokine profile was observed with the exception that the levels of complement component C5/C5a and TIMP-1 were very low while those of TNFα were detectable (Fig. 1, *C* and *D*). The increased levels of several inflammatory cytokines/chemokines

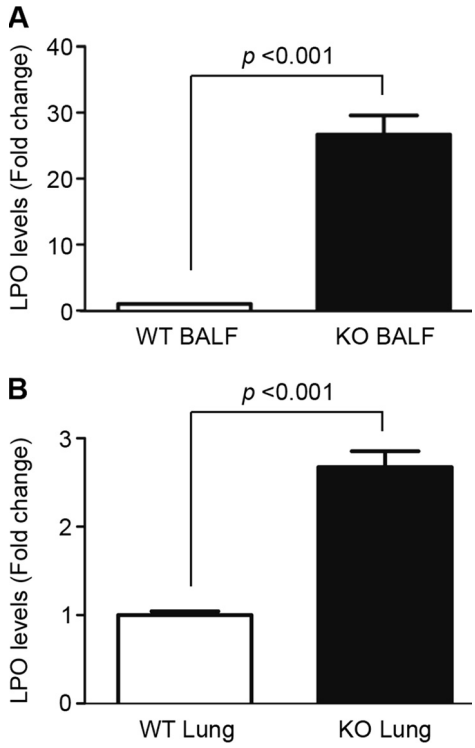

FIGURE 3. **LPO production in BALF and lung tissues.** LPO levels in the BALF (*A*) and lung lysates (*B*) were determined as described under "Experimental Procedures." The data in *Ig-Hepta*$^{-/-}$ (KO) mice are expressed relative to the WT mice. Values are means ± S.E. (*error bars*) from three mice.

and the accumulation of foamy AMs (27–29) suggest that local inflammation occurs in the alveoli of *Ig-Hepta*$^{-/-}$ mice.

ROS Accumulation in AMs of Ig-Hepta$^{-/-}$ *Mice*—Increased ROS production has been implicated in the development of emphysema (31, 32). Because AM is known to be the major source of ROS (33, 34), we examined ROS production in the AMs of *Ig-Hepta*$^{-/-}$ mice by staining with H_2DCFDA, a fluorogenic probe for intracellular ROS. Accumulation of ROS was observed in the cytoplasm of the AMs, which were double-labeled with the macrophage marker CD68 (Fig. 2, *A*, *C*, and *E*). The number of cells with positive H_2DCFDA staining increased with age (Fig. 2*G*). In contrast, less staining was observed in the AMs of WT mice (Fig. 2, *B*, *D*, and *F*). Furthermore, we observed that the levels of lipid hydroperoxide (LPO), a marker of oxidative stress, were significantly increased in BALF and lung tissue of *Ig-Hepta*$^{-/-}$ mice (Fig. 3). These results suggest that the deletion of the *Ig-Hepta* gene causes excessive ROS production by AMs and subsequent oxidative stress in the alveoli.

Activation of NF-κB in AMs of Ig-Hepta$^{-/-}$ *Mice*—ROS activate the redox-sensitive transcription factors involved in mediating inflammatory response, such as NF-κB (7). NF-κB is a heterodimer consisting of 50- and 65-kDa subunits (p50 and p65), and its inactive form is localized in the cytosol. Following degradation of the cellular NF-κB inhibitor IκB, active NF-κB translocates into the nucleus and promotes target gene transcription (35). Western blot analysis showed increased p65

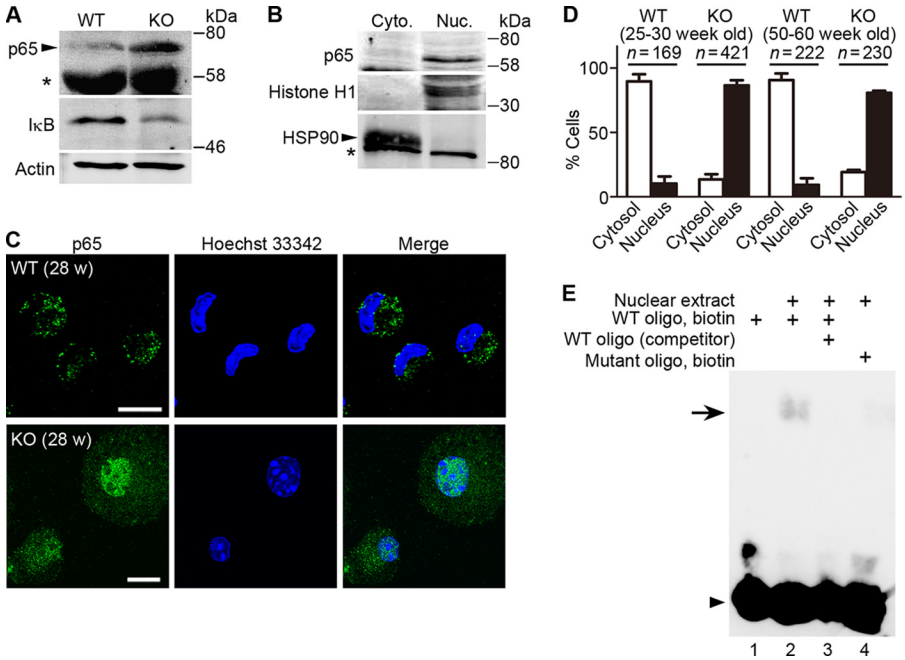

FIGURE 4. **NF-κB activation in the AM of *Ig-Hepta*$^{-/-}$ mice.** *A*, BALF was prepared from 60-week-old WT and *Ig-Hepta*$^{-/-}$ (KO) mice. Equal amounts of protein lysates (20 μg of protein each) were analyzed by Western blotting with antibodies against p65 (*top*), IκB (*middle*), and actin (for loading control; *bottom*). *, nonspecific immunoreactive bands. *B*, cytosolic (*left lane*) and nuclear fractions (*right lane*) of the *Ig-Hepta*$^{-/-}$ AMs (100 μg of proteins) were analyzed by Western blotting with antibodies against p65 (*top*), histone H1 (*middle*; a nuclear marker), and heat shock protein 90 (*bottom*; HSP90, a cytosolic marker). *, nonspecific immunoreactive bands. *C*, AMs were isolated from *Ig-Hepta*$^{-/-}$ (KO) and WT mice at 28 weeks at age. The AMs were stained with anti-p65 antibody (*green* in *left panels*) and Hoechst 33342 (*blue* in *middle panels*), and then observed with a confocal microscope. AMs of *Ig-Hepta*$^{-/-}$ mice often have enlarged, round nuclei and swollen cytoplasm, which are due to macrophage activation and excessive phagocytosis of surfactants (27–29). *Bars*, 25 μm. *D*, bar graphs represent the percentage of cells showing only p65 cytoplasmic staining (*open bar*) and those showing p65 nuclear staining or both (*filled bar*), which were quantified in randomly chosen views. Values are means ± S.E. (*error bars*) from three mice. *E*, biotin-labeled WT (*lanes 1–3*) and mutant NF-κB oligonucleotides (*lanes 4*) were incubated in the presence or absence of nuclear extracts of the *Ig-Hepta*$^{-/-}$ AMs. For a control experiment, excess unlabeled WT oligonucleotides were added to the reaction mixture as a competitor (*lane 3*). The oligonucleotides were subjected to polyacrylamide gel electrophoresis and then detected with horseradish-conjugated streptavidin. The *arrowhead* and *arrow* indicate bands corresponding to free biotin-labeled oligonucleotides and mobility shift of oligonucleotides, respectively.

expression and decreased IκB-α expression in the AMs of *Ig-Hepta*$^{-/-}$ mice (Fig. 4*A*). In addition, subcellular fractionation showed the nuclear localization of p65 in the AMs of *Ig-Hepta*$^{-/-}$ mice (Fig. 4*B*). Consistent with these results, immunofluorescent confocal microscopy showed that the AMs of *Ig-Hepta*$^{-/-}$ mice were strongly stained with anti-p65 antibody compared with those of WT mice (Fig. 4*C*). In addition, the nuclear localization of p65 was observed in ~83% of the AMs in *Ig-Hepta*$^{-/-}$ mice, whereas it was seen in only 10% of the AMs in WT mice (Fig. 4*D*). To determine the activity of NF-κB, EMSA was performed using nuclear extracts from the AMs of *Ig-Hepta*$^{-/-}$ mice. Mobility shift of a consensus NF-κB oligonucleotide was observed in the presence of the nuclear extracts (Fig. 4*E*, *lane 2*, *arrow*). This shift was abolished when a point mutation was introduced into the NF-κB-binding sequence (Fig. 4*E*, *lane 4*). These results suggest that NF-κB is highly activated in the AMs of *Ig-Hepta*$^{-/-}$ mice.

Increased Expression and Activity of MMPs in the Lung of Ig-Hepta$^{-/-}$ *Mice*—It has been shown that increased levels of MMP-2, MMP-9, and MMP-12 are associated with emphysema in human and animal models (36–38). We have previously reported that MMP-12 expression is elevated in the lung of *Ig-Hepta*$^{-/-}$ mice (27). We therefore examined the expression levels of MMP-2 and MMP-9 by Western blotting. Expression of MMP-2 and MMP-9 was very low or undetectable in the BALF of WT mice, whereas their levels were markedly increased in the BALF of *Ig-Hepta*$^{-/-}$ mice (Fig. 5*A*). In addition, quantitative real-time PCR analysis showed that *Mmp2* and *Mmp9* expression were significantly increased in the AMs of *Ig-Hepta*$^{-/-}$ mice (Fig. 5*B*). Furthermore, gelatin zymography studies showed that their gelatinase activity are also increased in the BALF from *Ig-Hepta*$^{-/-}$ mice; there were three major gelatinase bands corresponding to MMP-2, MMP-9, and pro-MMP-9 at positions of ~64, 82, and 97 kDa, respectively (Fig. 5*C*). To investigate whether the increased MMP expression is mediated by oxidative stress-induced NF-κB activation, the AMs of *Ig-Hepta*$^{-/-}$ mice were treated with pyrrolidine dithiocarbamate, an antioxidant, and the activity of released MMPs was then analyzed by gelatin zymography. Treatments with pyrrolidine dithiocarbamate resulted in a marked decrease in the MMP activity (Fig. 5*D*). Similar results were obtained when the AMs were treated with another antioxidant, *N*-acetyl-L-cysteine (*NAC* in Fig. 5*E*), or with the NF-κB inhibitors parthenolide (Fig. 5*F*) and BAY 11-7082 (Fig. 5*G*). These results suggest that the AMs of *Ig-Hepta*$^{-/-}$ mice promote MMP production through ROS-induced NF-κB activation.

Increased Cytokine and Chemokine Expression in the Lung of Embryonic Ig-Hepta$^{-/-}$ *Mice*—It has been reported that Ig-Hepta expression is induced in mouse lung at 18 dpc, whereas accumulation of pulmonary surfactant initiates after birth (27, 28). We observed that expression levels of F8/40 (a macrophage marker), *Mmp2*, and *Mmp9* are comparable in the lung between WT and *Ig-Hepta*$^{-/-}$ mice at 18.5 dpc (Fig. 6, *A* and *B*), suggesting that AM accumulation and activation do not occur during embryonic development. When the cytokine/chemokine profile was analyzed using 18.5-dpc lung lysates, increased expression of MCP-1 was detected in *Ig-Hepta*$^{-/-}$ mice (Fig. 6, *C* and *D*). Other factors, such as CCL1, IL-7, IL-13, and CCL12, also increased, albeit at very low expression levels (Fig. 6, *C* and *D*). We failed to analyze the cytokine/chemokine profile of BALF and AMs due to technical difficulty in obtaining lavage fluid from very small lungs. These results suggest that deletion of Ig-Hepta promotes the expression of proinflammatory mediators in embryonic lungs prior to macrophage activation.

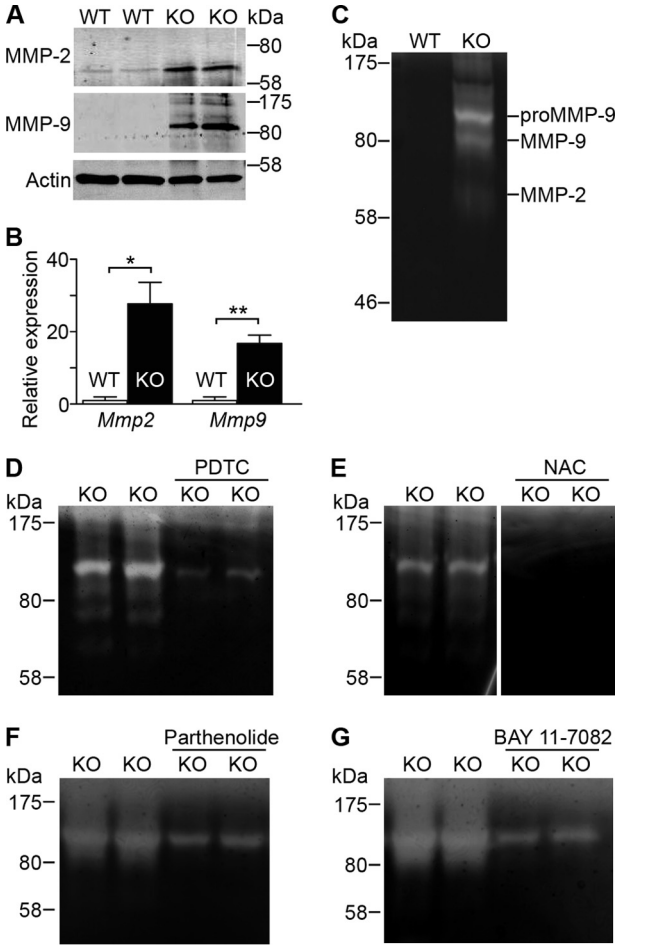

FIGURE 5. **Up-regulation of MMPs in the AMs of *Ig-Hepta*$^{-/-}$ mice.** *A*, Western blot analysis was performed on the BALF (20 μg of protein each) prepared from 12-week-old WT and *Ig-Hepta*$^{-/-}$ (KO) mice. The protein bands corresponding to MMP-2, MMP-9, and β-actin are shown. *B*, quantitative real-time PCR was performed to determine the expression levels of *Mmp2* and *Mmp9* in AMs of 12-week-old WT and *Ig-Hepta*$^{-/-}$ (KO) mice. The data from three independent experiments were normalized to the levels of *Gapdh* and are expressed relative to the levels in WT mice. *, $p < 0.05$; **, $p < 0.005$ (Student's *t* test). *C*, the gelatinase activity of MMP-2 and MMP-9 in the BALF was assessed by gelatin zymography. *D–G*, AMs were isolated from *Ig-Hepta*$^{-/-}$ mice and treated with 200 μM pyrrolidine dithiocarbamate (*PDTC*) (*D*), 20 mM *N*-acetyl-L-cysteine (*NAC*) (*E*), 50 μM parthenolide (*F*), or 20 μM BAY 11-7082 (*G*). The activities of MMP-2 and MMP-9 secreted from the AMs were determined by gelatin zymography. *Error bars*, S.E.

DISCUSSION

Recent studies have shown that targeted disruption of Ig-Hepta in mice results in abnormal lung structure with enlarged alveoli and in progressive accumulation of pulmonary surfactant and AMs (27–29). These abnormalities are similar to those seen in patients and animal models with emphysema (21, 39, 40), but the underlying mechanism of pathogenesis has not been elucidated. Because AMs have been shown to play a pivotal role in the pathogenesis of emphysema, we determined and

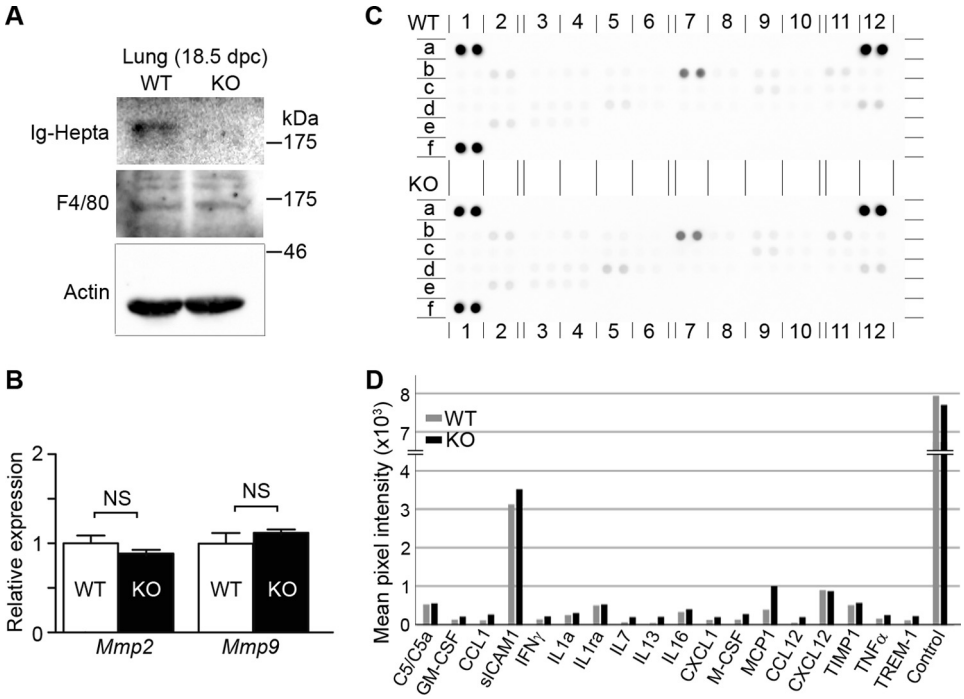

FIGURE 6. **Increased cytokine and chemokine expression in the lung of embryonic *Ig-Hepta*$^{-/-}$ mice.** *A*, Western blot analysis was performed on lung lysates prepared from WT and *Ig-Hepta*$^{-/-}$ (KO) mice at 18.5 dpc (60 μg of protein each). The protein bands corresponding to Ig-Hepta, F8/40, and β-actin are shown. *B*, the expression levels of *Mmp2* and *Mmp9* in embryonic lungs (18 dpc) were analyzed by quantitative real-time PCR. The data from three independent experiments were normalized to the levels of *Gapdh* and are expressed relative to the levels in WT mice. *NS*, no significant difference (Student's *t* test). *C*, Proteome Profiler Mouse Cytokine Arrays were used to detect cytokines and chemokines present in lung lysates prepared from three embryonic WT (*top*) or *Ig-Hepta*$^{-/-}$ (KO; *bottom*) mice (18.5 dpc). The identity of each spot is indicated in the legend to Fig. 1. *D*, the signal intensity of each spot was quantified and shown in the bar graph. *Gray bar*, WT mice. *Filled bar*, *Ig-Hepta*$^{-/-}$ (KO) mice.

compared ROS accumulation, NF-κB activation, and MMP production in the AMs of wild-type and *Ig-Hepta*$^{-/-}$ mice. Our results showed that the AMs of *Ig-Hepta*$^{-/-}$ mice have response profiles similar to those observed in emphysema.

An extensive accumulation of the AMs occurs in the alveoli of *Ig-Hepta*$^{-/-}$ mice as early as 3 weeks of age and progressively increases thereafter (27, 28). Most AMs are enlarged and become foamy with lipid-laden phagosomes due to extensive uptake of surfactant lipids (27–29). The increased levels of MCP-1/CCL2, CCL3, and complement component C5a (Fig. 1) are likely to promote recruitment of monocytes/macrophages within the alveoli. In addition to these morphological abnormalities, we showed increased ROS levels in the AMs of both young and old *Ig-Hepta*$^{-/-}$ mice (Fig. 2). ROS are increasingly recognized as important mediators of fundamental cellular functions, such as cell growth and differentiation, cell signaling, stress response, and apoptosis (41, 42). However, their excessive production is known to lead to oxidative stress resulting in tissue injury. Therefore, Ig-Hepta may have an antioxidant role in maintaining ROS homeostasis and protect the lung tissue from oxidative stress. The accumulation of LPO in the lung tissue (Fig. 3) suggests that the lung parenchyma is exposed to oxidative stress. The increased ROS levels are, however, unlikely to reflect a direct effect of *Ig-Hepta* deletion because Ig-Hepta expression is not detected in AMs (27, 29). This is supported by the findings by Yang *et al.* (29) that the phenotype observed in AMs is not autonomous but rather determined by the lung microenvironment of *Ig-Hepta*$^{-/-}$ mice. SP-D knockout mice develop emphysema with an increased number of foamy macrophages, excess surfactant, and overproduction of ROS (24). The similarities in phenotypes between Ig-Hepta and SP-D knock-out mice lead us to speculate that increased levels of surfactant components may stimulate AMs to produce ROS. In the development of atherosclerosis, the scavenger receptors for oxidized low density lipoproteins (LDLs), such as CD36 and SR-A (scavenger receptor-A), promote cholesterol uptake by tissue macrophages, leading to foamy cell formation and ROS production (43). A large amount of LPO in the BALF (Fig. 3) suggests that oxidized (surfactant) lipids may be incorporated into the AMs and enhance ROS generation. Taking into account the fact that the alveolar type II cells also produce and release ROS (44, 45), another possibility would be to assume that deletion of Ig-Hepta leads to imbalanced ROS homeostasis in the alveolar type II cells, which promotes ROS release toward AMs as well as surfactant lipids.

Accumulated evidence has shown that ROS can initiate inflammatory responses in the lung though the activation of the redox-sensitive transcription factor NF-κB (5, 24, 46). In support of the close relationship between ROS and NF-κB activation, increased nuclear expression of NF-κB was detected in the AMs of *Ig-Hepta*$^{-/-}$ mice (Fig. 4). In addition to the previous finding of increased MMP-12 expression (27), we found increased levels and activity of MMP-2 and MMP-9 in the BALF from *Ig-Hepta*$^{-/-}$ mice (Fig. 5). This phenomenon is closely similar to that observed in COPD patients and in mice with emphysema induced by cigarette smoke or gene knockout (23, 47–50). Taking account of the fact that the promoter regions of the *MMP2* and *MMP9* genes contain binding sites

for NF-κB for their transcriptional regulation (8, 9), the increased expression of MMP-2 and MMP-9 in *Ig-Hepta*$^{-/-}$ mice is likely to be mediated through ROS-dependent NF-κB activation. Because MMP-12 expression is also regulated by ROS and NF-κB (51, 52), the up-regulation of MMP-12 observed in *Ig-Hepta*$^{-/-}$ mice may be mediated via a similar mechanism. MMP-2 and MMP-9 are known to degrade type IV collagen and gelatin, which are major components of the extracellular matrix (53–55). Their excess activity has been thought to contribute to the development of emphysema through extensive destruction of the extracellular matrix and remodeling of lung parenchyma (54, 56, 57). Therefore, we propose that the alveolar enlargement in *Ig-Hepta*$^{-/-}$ may result from the overactivation of the MMPs, which causes alveolar tissue destruction and remodeling.

It is still unknown how the local inflammatory response is initiated. We found that increased expression of cytokines and chemokines occurs in the lungs of *Ig-Hepta*$^{-/-}$ mice at 18.5 dpc, in which no significant accumulation or activation of AMs was observed (Fig. 6). Bridges *et al.* (28) have reported that P2RY2, a purinergic receptor, is up-regulated in the alveolar type II cells of embryonic *Ig-Hepta*$^{-/-}$ mice at 18.5 dpc. They hypothesized that activation of P2RY2 signaling stimulates surfactant release from the alveolar type II cells after birth. P2RY2 is known to induce proinflammatory cytokines and chemokines, including MCP-1, from several types of cells, such as epithelial cells, fibroblasts, myocytes, and macrophages (58–61). In addition, the alveolar type II cells have the ability to recruit and activate AMs by secreting MCP-1 (62, 63). Therefore, it is possible that activation of P2RY2 signaling by Ig-Hepta deletion might promote the release of MCP-1 and other proinflammatory mediators from the alveolar type II cells, thereby leading to attraction and activation of AMs.

In conclusion, *Ig-Hepta*$^{-/-}$ mice exhibit emphysema-like symptoms, in which AMs are activated and release MMPs through ROS-mediated NF-κB activation. The macrophage activation is likely to be mediated by MCP-1 induced by Ig-Hepta deletion, but the underlying mechanism, including Ig-Hepta-mediated signaling, should be elucidated in future studies. Our findings suggest that Ig-Hepta bears the responsibility for ensuring homeostasis of the internal environment of the alveoli, such as surfactant homeostasis, to prevent macrophage activation and emphysema. Therefore, we propose that *Ig-Hepta*$^{-/-}$ mice are a useful model to gain insights into the pathogenesis and treatment of emphysema.

Acknowledgments—We thank Fumimasa Kubo and Noriko Isoyama for maintaining mice and Yuriko Ishii for secretarial assistance.

REFERENCES

1. Mannino, D. M., and Buist, A. S. (2007) Global burden of COPD: risk factors, prevalence, and future trends. *Lancet* **370,** 765–773
2. Taraseviciene-Stewart, L., and Voelkel, N. F. (2008) Molecular pathogenesis of emphysema. *J. Clin. Invest.* **118,** 394–402
3. Finkelstein, R., Fraser, R. S., Ghezzo, H., and Cosio, M. G. (1995) Alveolar inflammation and its relation to emphysema in smokers. *Am. J. Respir. Crit. Care Med.* **152,** 1666–1672
4. Churg, A., Wang, R. D., Tai, H., Wang, X., Xie, C., and Wright, J. L. (2004) Tumor necrosis factor-α drives 70% of cigarette smoke-induced emphysema in the mouse. *Am. J. Respir. Crit. Care Med.* **170,** 492–498
5. Rahman, I., and Adcock, I. M. (2006) Oxidative stress and redox regulation of lung inflammation in COPD. *Eur. Respir. J.* **28,** 219–242
6. van Zoelen, M. A., Verstege, M. I., Draing, C., de Beer, R., van't Veer, C., Florquin, S., Bresser, P., van der Zee, J. S., te Velde, A. A., von Aulock, S., and van der Poll, T. (2011) Endogenous MCP-1 promotes lung inflammation induced by LPS and LTA. *Mol. Immunol.* **48,** 1468–1476
7. Sen, C. K., and Packer, L. (1996) Antioxidant and redox regulation of gene transcription. *FASEB J.* **10,** 709–720
8. Lee, S. J., Bae, S. S., Kim, K. H., Lee, W. S., Rhim, B. Y., Hong, K. W., and Kim, C. D. (2007) High glucose enhances MMP-2 production in adventitial fibroblasts via Akt1-dependent NF-κB pathway. *FEBS Lett.* **581,** 4189–4194
9. Bond, M., Chase, A. J., Baker, A. H., and Newby, A. C. (2001) Inhibition of transcription factor NF-κB reduces matrix metalloproteinase-1, -3 and -9 production by vascular smooth muscle cells. *Cardiovasc. Res.* **50,** 556–565
10. Munaut, C., Salonurmi, T., Kontusaari, S., Reponen, P., Morita, T., Foidart, J. M., and Tryggvason, K. (1999) Murine matrix metalloproteinase 9 gene: 5′-upstream region contains cis-acting elements for expression in osteoclasts and migrating keratinocytes in transgenic mice. *J. Biol. Chem.* **274,** 5588–5596
11. Pérez-Rial, S., del Puerto-Nevado, L., Terrón-Expósito, R., Girón-Martínez, Á., González-Mangado, N., and Peces-Barba, G. (2013) Role of recently migrated monocytes in cigarette smoke-induced lung inflammation in different strain of mice. *PLoS One* **8,** e72975
12. Vu, T. H., and Werb, Z. (2000) Matrix metalloproteinases: effectors of development and normal physiology. *Genes Dev.* **14,** 2123–2133
13. Shapiro, S. D. (2002) Proteinases in chronic obstructive pulmonary disease. *Biochem. Soc. Trans.* **30,** 98–102
14. Churg, A., Cosio, M., and Wright, J. L. (2008) Mechanisms of cigarette smoke-induced COPD: insights from animal models. *Am. J. Physiol. Lung Cell Mol. Physiol.* **294,** L612–L631
15. Wright, J. L., Cosio, M., and Churg, A. (2008) Animal models of chronic obstructive pulmonary disease. *Am. J. Physiol. Lung Cell Mol. Physiol.* **295,** L1–L15
16. Rooney, S. A., Young, S. L., and Mendelson, C. R. (1994) Molecular and cellular processing of lung surfactant. *FASEB J.* **8,** 957–967
17. Gilliard, N., Heldt, G. P., Loredo, J., Gasser, H., Redl, H., Merritt, T. A., and Spragg, R. G. (1994) Exposure of the hydrophobic components of porcine lung surfactant to oxidant stress alters surface tension properties. *J. Clin. Invest.* **93,** 2608–2615
18. Müller, B., Seifart, C., and Barth, P. J. (1998) Effect of air pollutants on the pulmonary surfactant system. *Eur. J. Clin. Invest.* **28,** 762–777
19. Andersson, S., Kheiter, A., and Merritt, T. A. (1999) Oxidative inactivation of surfactants. *Lung* **177,** 179–189
20. Glasser, S. W., Detmer, E. A., Ikegami, M., Na, C. L., Stahlman, M. T., and Whitsett, J. A. (2003) Pneumonitis and emphysema in sp-C gene targeted mice. *J. Biol. Chem.* **278,** 14291–14298
21. Mechri, M., Epaud, R., Emond, S., Coulomb, A., Jaubert, F., Tarrant, A., Feldmann, D., Flamein, F., Clement, A., de Blic, J., Taam, R. A., Brunelle, F., and le Pointe, H. D. (2010) Surfactant protein C gene (SFTPC) mutation-associated lung disease: high-resolution computed tomography (HRCT) findings and its relation to histological analysis. *Pediatr. Pulmonol.* **45,** 1021–1029
22. Maguire, J. A., Mulugeta, S., and Beers, M. F. (2011) Endoplasmic reticulum stress induced by surfactant protein C BRICHOS mutants promotes proinflammatory signaling by epithelial cells. *Am. J. Respir. Cell Mol. Biol.* **44,** 404–414
23. Wert, S. E., Yoshida, M., LeVine, A. M., Ikegami, M., Jones, T., Ross, G. F., Fisher, J. H., Korfhagen, T. R., and Whitsett, J. A. (2000) Increased metalloproteinase activity, oxidant production, and emphysema in surfactant protein D gene-inactivated mice. *Proc. Natl. Acad. Sci. U.S.A.* **97,** 5972–5977
24. Yoshida, M., Korfhagen, T. R., and Whitsett, J. A. (2001) Surfactant protein D regulates NF-κB and matrix metalloproteinase production in alveolar macrophages via oxidant-sensitive pathways. *J. Immunol.* **166,** 7514–7519
25. Besnard, V., Matsuzaki, Y., Clark, J., Xu, Y., Wert, S. E., Ikegami, M., Stahlman, M. T., Weaver, T. E., Hunt, A. N., Postle, A. D., and Whitsett,

J. A. (2010) Conditional deletion of Abca3 in alveolar type II cells alters surfactant homeostasis in newborn and adult mice. *Am. J. Physiol. Lung Cell Mol. Physiol.* **298,** L646–L659
26. Abe, J., Suzuki, H., Notoya, M., Yamamoto, T., and Hirose, S. (1999) Ig-hepta, a novel member of the G protein-coupled hepta-helical receptor (GPCR) family that has immunoglobulin-like repeats in a long N-terminal extracellular domain and defines a new subfamily of GPCRs. *J. Biol. Chem.* **274,** 19957–19964
27. Fukuzawa, T., Ishida, J., Kato, A., Ichinose, T., Ariestanti, D. M., Takahashi, T., Ito, K., Abe, J., Suzuki, T., Wakana, S., Fukamizu, A., Nakamura, N., and Hirose, S. (2013) Lung surfactant levels are regulated by Ig-Hepta/GPR116 by monitoring surfactant protein D. *PLoS One* **8,** e69451
28. Bridges, J. P., Ludwig, M. G., Mueller, M., Kinzel, B., Sato, A., Xu, Y., Whitsett, J. A., and Ikegami, M. (2013) Orphan G protein-coupled receptor GPR116 regulates pulmonary surfactant pool size. *Am. J. Respir. Cell Mol. Biol.* **49,** 348–357
29. Yang, M. Y., Hilton, M. B., Seaman, S., Haines, D. C., Nagashima, K., Burks, C. M., Tessarollo, L., Ivanova, P. T., Brown, H. A., Umstead, T. M., Floros, J., Chroneos, Z. C., and St Croix, B. (2013) Essential regulation of lung surfactant homeostasis by the orphan G protein-coupled receptor GPR116. *Cell Rep.* **3,** 1457–1464
30. Ikegami, M., Whitsett, J. A., Jobe, A., Ross, G., Fisher, J., and Korfhagen, T. (2000) Surfactant metabolism in SP-D gene-targeted mice. *Am. J. Physiol. Lung Cell Mol. Physiol.* **279,** L468–L476
31. Yao, H., Edirisinghe, I., Yang, S. R., Rajendrasozhan, S., Kode, A., Caito, S., Adenuga, D., and Rahman, I. (2008) Genetic ablation of NADPH oxidase enhances susceptibility to cigarette smoke-induced lung inflammation and emphysema in mice. *Am. J. Pathol.* **172,** 1222–1237
32. Yao, H., Yang, S. R., Kode, A., Rajendrasozhan, S., Caito, S., Adenuga, D., Henry, R., Edirisinghe, I., and Rahman, I. (2007) Redox regulation of lung inflammation: role of NADPH oxidase and NF-κB signalling. *Biochem. Soc. Trans.* **35,** 1151–1155
33. Haugen, T. S., Skjønsberg, O. H., Kähler, H., and Lyberg, T. (1999) Production of oxidants in alveolar macrophages and blood leukocytes. *Eur. Respir. J.* **14,** 1100–1105
34. Doelman, C. J., and Bast, A. (1990) Oxygen radicals in lung pathology. *Free Radic. Biol. Med.* **9,** 381–400
35. Baldwin, A. S., Jr. (1996) The NF-κB and IκB proteins: new discoveries and insights. *Annu. Rev. Immunol.* **14,** 649–683
36. Baraldo, S., Bazzan, E., Zanin, M. E., Turato, G., Garbisa, S., Maestrelli, P., Papi, A., Miniati, M., Fabbri, L. M., Zuin, R., and Saetta, M. (2007) Matrix metalloproteinase-2 protein in lung periphery is related to COPD progression. *Chest* **132,** 1733–1740
37. Churg, A., Wang, R., Wang, X., Onnervik, P. O., Thim, K., and Wright, J. L. (2007) Effect of an MMP-9/MMP-12 inhibitor on smoke-induced emphysema and airway remodelling in guinea pigs. *Thorax* **62,** 706–713
38. Molet, S., Belleguic, C., Lena, H., Germain, N., Bertrand, C. P., Shapiro, S. D., Planquois, J. M., Delaval, P., and Lagente, V. (2005) Increase in macrophage elastase (MMP-12) in lungs from patients with chronic obstructive pulmonary disease. *Inflamm. Res.* **54,** 31–36
39. Deacu, M., Tofolean, D. E., Boşoteanu, M., Aşchie, M., and Bulbuc, I. (2012) Pulmonary alveolar lipoproteinosis associated with emphysematous areas. *Rom. J. Morphol. Embryol.* **53,** 173–177
40. Hirama, N., Shibata, Y., Otake, K., Machiya, J., Wada, T., Inoue, S., Abe, S., Takabatake, N., Sata, M., and Kubota, I. (2007) Increased surfactant protein-D and foamy macrophages in smoking-induced mouse emphysema. *Respirology* **12,** 191–201
41. Valko, M., Rhodes, C. J., Moncol, J., Izakovic, M., and Mazur, M. (2006) Free radicals, metals and antioxidants in oxidative stress-induced cancer. *Chem. Biol. Interact.* **160,** 1–40
42. Ray, P. D., Huang, B. W., and Tsuji, Y. (2012) Reactive oxygen species (ROS) homeostasis and redox regulation in cellular signaling. *Cell. Signal.* **24,** 981–990
43. Moore, K. J., and Freeman, M. W. (2006) Scavenger receptors in atherosclerosis: beyond lipid uptake. *Arterioscler. Thromb. Vasc. Biol.* **26,** 1702–1711
44. Kinnula, V. L., Everitt, J. I., Whorton, A. R., and Crapo, J. D. (1991) Hydrogen peroxide production by alveolar type II cells, alveolar macrophages, and endothelial cells. *Am. J. Physiol.* **261,** L84–L91
45. Bedard, K., and Krause, K. H. (2007) The NOX family of ROS-generating NADPH oxidases: physiology and pathophysiology. *Physiol. Rev.* **87,** 245–313
46. Li, N., and Karin, M. (1999) Is NF-κB the sensor of oxidative stress? *FASEB J.* **13,** 1137–1143
47. Ohnishi, K., Takagi, M., Kurokawa, Y., Satomi, S., and Konttinen, Y. T. (1998) Matrix metalloproteinase-mediated extracellular matrix protein degradation in human pulmonary emphysema. *Lab. Invest.* **78,** 1077–1087
48. Segura-Valdez, L., Pardo, A., Gaxiola, M., Uhal, B. D., Becerril, C., and Selman, M. (2000) Upregulation of gelatinases A and B, collagenases 1 and 2, and increased parenchymal cell death in COPD. *Chest* **117,** 684–694
49. Vernooy, J. H., Lindeman, J. H., Jacobs, J. A., Hanemaaijer, R., and Wouters, E. F. (2004) Increased activity of matrix metalloproteinase-8 and matrix metalloproteinase-9 in induced sputum from patients with COPD. *Chest* **126,** 1802–1810
50. Wright, J. L., Tai, H., Wang, R., Wang, X., and Churg, A. (2007) Cigarette smoke upregulates pulmonary vascular matrix metalloproteinases via TNF-α signaling. *Am. J. Physiol. Lung Cell Mol. Physiol.* **292,** L125–L133
51. Lavigne, M. C., and Eppihimer, M. J. (2005) Cigarette smoke condensate induces MMP-12 gene expression in airway-like epithelia. *Biochem. Biophys. Res. Commun.* **330,** 194–203
52. Kim, M. J., Nepal, S., Lee, E. S., Jeong, T. C., Kim, S. H., and Park, P. H. (2013) Ethanol increases matrix metalloproteinase-12 expression via NADPH oxidase-dependent ROS production in macrophages. *Toxicol. Appl. Pharmacol.* **273,** 77–89
53. Mackay, A. R., Hartzler, J. L., Pelina, M. D., and Thorgeirsson, U. P. (1990) Studies on the ability of 65-kDa and 92-kDa tumor cell gelatinases to degrade type IV collagen. *J. Biol. Chem.* **265,** 21929–21934
54. Chakrabarti, S., and Patel, K. D. (2005) Matrix metalloproteinase-2 (MMP-2) and MMP-9 in pulmonary pathology. *Exp. Lung Res.* **31,** 599–621
55. Löffek, S., Schilling, O., and Franzke, C. W. (2011) Series "matrix metalloproteinases in lung health and disease": biological role of matrix metalloproteinases: a critical balance. *Eur. Respir. J.* **38,** 191–208
56. Corbel, M., Boichot, E., and Lagente, V. (2000) Role of gelatinases MMP-2 and MMP-9 in tissue remodeling following acute lung injury. *Braz. J. Med. Biol. Res.* **33,** 749–754
57. Foronjy, R., Nkyimbeng, T., Wallace, A., Thankachen, J., Okada, Y., Lemaitre, V., and D'Armiento, J. (2008) Transgenic expression of matrix metalloproteinase-9 causes adult-onset emphysema in mice associated with the loss of alveolar elastin. *Am. J. Physiol. Lung Cell Mol. Physiol.* **294,** L1149–L1157
58. Kruse, R., Demirel, I., Säve, S., and Persson, K. (2014) IL-8 and global gene expression analysis define a key role of ATP in renal epithelial cell responses induced by uropathogenic bacteria. *Purinergic Signal.* **10,** 499–508
59. Braun, O. O., Lu, D., Aroonsakool, N., and Insel, P. A. (2010) Uridine triphosphate (UTP) induces profibrotic responses in cardiac fibroblasts by activation of P2Y2 receptors. *J. Mol. Cell Cardiol.* **49,** 362–369
60. Schuchardt, M., Prüfer, J., Prüfer, N., Wiedon, A., Huang, T., Chebli, M., Jankowski, V., Jankowski, J., Schäfer-Korting, M., Zidek, W., van der Giet, M., and Tölle, M. (2011) The endothelium-derived contracting factor uridine adenosine tetraphosphate induces $P2Y_2$-mediated pro-inflammatory signaling by monocyte chemoattractant protein-1 formation. *J. Mol. Med.* **89,** 799–810
61. Stokes, L., and Surprenant, A. (2007) Purinergic P2Y2 receptors induce increased MCP-1/CCL2 synthesis and release from rat alveolar and peritoneal macrophages. *J. Immunol.* **179,** 6016–6023
62. Amano, H., Morimoto, K., Senba, M., Wang, H., Ishida, Y., Kumatori, A., Yoshimine, H., Oishi, K., Mukaida, N., and Nagatake, T. (2004) Essential contribution of monocyte chemoattractant protein-1/C-C chemokine ligand-2 to resolution and repair processes in acute bacterial pneumonia. *J. Immunol.* **172,** 398–409
63. Kannan, S., Huang, H., Seeger, D., Audet, A., Chen, Y., Huang, C., Gao, H., Li, S., and Wu, M. (2009) Alveolar epithelial type II cells activate alveolar macrophages and mitigate *P. aeruginosa* infection. *PLoS One* **4,** e4891